IET Microwaves, Antennas & Propagation

Research Article

IET Journals
The Institution of Engineering and Technology

Pedestal substrate integrated waveguide resonators and filters

ISSN 1751-8725
Received on 12th February 2016
Revised 8th November 2016
Accepted on 6th December 2016
E-First on 10th March 2017
doi: 10.1049/iet-map.2016.0120
www.ietdl.org

Shamim O. Nassar[1], *Petrie Meyer*[1] ✉

[1]*Department of E&E Engineering, University of Stellenbosch, Private Bag X1, 7602 Matieland, South Africa*
✉ *E-mail: pmeyer@sun.ac.za*

Abstract: A new substrate integrated waveguide resonator in the form of a square- or cross-shaped pedestal is proposed. The structure is developed from T-shaped ridge waveguides, and utilises the mode separation characteristics of this type of guide to achieve wider spacing between the first two resonances, as well as miniaturisation of the resonator. Two fourth-order X-band filters, one with cross-coupling, are designed using, respectively, square- and cross-shaped pedestal resonators, and validated by simulation and measurement.

1 Introduction

Even though waveguide technology is the oldest implementation of microwave filters, it still offers superior performance in terms of loss and power handling, at the cost of large physical size and weight. However, waveguide filters fundamentally suffer from the problem of limited stopband width, due to the propagation of higher order modes. Currently, microwave filters with wide stopbands are often required in systems where spurious responses are problematic. The most widely used waveguide structure to achieve this is the classical waffle-iron waveguide filter, but for narrow bandwidth filters requiring wide stopbands, waveguide is often not the optimal choice. Instead, cavity or planar combline filters with resonators shorter than a quarter wavelength are often used, with variations employing very high capacitive end-loading achieving stopbands of up to $4.3f_0$ [1]. In planar technology, recent years have also seen a number of techniques using sub-wavelength resonators underneath or in close proximity of resonators to create bandgap regions [2].

In waveguide, the classical ridge waveguide filter does however also offer a solution to this problem. By introducing a ridge structure into a waveguide, the cut-off frequency of the fundamental mode of the waveguide is lowered, increasing the frequency separation between the cut-off frequencies of the first two modes. Also, for the same outer dimensions, the guide can operate in the fundamental mode at much lower frequencies, resulting in circuit miniaturisation. Ridge waveguides find wide application in various radio frequency and microwave component designs [3–6], and their properties are well defined in literature [7–11].

In recent years, waveguide implementations in planar dielectric substrates have become popular, with substrate integrated waveguide (SIW) emerging as a widely used technology [12]. These structures realise effective dielectric filled waveguides by the use of rows of vias between the two ground planes on either side of a high-frequency substrate, and are cost-effective, lightweight, and offer easy integration with planar structures through several well-defined transitions [13]. As SIW closely mimics actual waveguide behaviour, the problem of higher order modes is however also present, resulting in limited pass-band separation. One approach to solve this has been that of Salehi and Mehrshahi [14], who use SIW resonators of mixed size, loaded with slots, to achieve pass-band separations of up to 1:2. Other approaches include the patterning of one of the SIW ground planes to create a series of sub-wavelength resonators which loads the main waveguides [15, 16]. Both these classes of solution however result in structures with unbounded fields.

This paper proposes a new type of structure, denoted as *pedestal resonators*, to both address the problem of spurious responses in SIW and to reduce resonator size. These resonators are based on the combination of SIW technology with the concepts of ridge waveguide, and offer very attractive possibilities for creating electrically closed, small, low-cost, and lightweight filters with wide stopbands. The resonators feature either rectangular or cross-shaped flat conductors on a single or a set of vias, positioned centrally inside each SIW cavity. Both resonators show increased spacing between the first two resonances when compared with normal or SIW guides, and in comparison with [14–16], a significant reduction in resonator size. In filter applications, the proposed resonators do not suppress unwanted resonances at specific frequencies as [14–16] realise through bandgap regions and/or slot resonances, but rather utilise the modal separation of the ridge guide to prevent these waves from propagating at all.

The paper discusses the characteristics of the two resonators in comparison to standard SIW, stripline, and ring resonators. Two fourth-order filters are designed, one at $f_0 = 9.1$ GHz and one at $f_0 = 7$ GHz, using, respectively, the cross-shaped pedestal resonator and the square-topped pedestal resonator, both on standard Rogers RO4003 substrate. Both filters achieve pass-band spacings of at least 1:2, with footprints of smaller than 19×19 mm.

2 T-ridge SIW

As the proposed resonators are developed from the basis of ridge waveguides, specifically an SIW implementation featuring a wide centre conductor, the characteristics of such a guide are first presented. Ridge waveguide implementations in SIW are well documented, with notably Bozzi *et al.* [17] presenting results for a number of cases, including those where the ridge is made up of unconnected vias in the longitudinal direction (*ridge SIW*), and where these vias are connected with a thin metal shim running the length of the structure (*modified ridge SIW*). The latter case especially showed good performance, yielding many of the same advantages as normal ridge waveguide. However, the case of SIW ridge waveguide with a centre conductor much wider than the diameter of the vias making up the vertical ridge, has not yet been investigated.

The structure of SIW, having discontinuous longitudinal boundaries, complicates basic analysis such as the determination of cut-off frequencies. However, it has been shown that the normal guide is an excellent approximation for SIW, given that certain dimensional relationships are adhered to. In the following, solid-wall waveguides with cross-sections independent of the longitudinal direction are therefore used to illustrate the cut-off

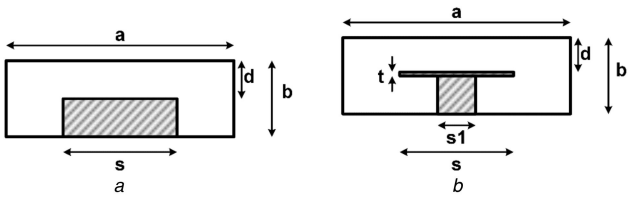

Fig. 1 *Waveguide cross-sections*
(a) Ridge guide, ***(b)*** T-ridge guide

behaviour of the basic building block of the proposed resonators, i.e. the T-ridge guide.

The cross-sections of normal ridge waveguide and T-ridge waveguide are shown in Fig. 1.

As a benchmark, we note that the cut-off frequency of the first mode in a conventional rectangular waveguide with the dimensions $a = 7.47$ mm and $b = 1.6$ mm, filled with a dielectric material with a relative permittivity of 3.38, is 10.64 GHz. A number of analyses of the two structures in Fig. 1 can now be used to compare the performance against each other, and a normal guide. In all cases, the two-dimensional (2D) port solver of CST Microwave Studio is used to calculate the cut-off frequencies. The dimensions of interest are the gap size, d, in relation to the waveguide height, b, and the ridge width, s. Also of interest is the T-ridge leg width, $s1$.

Evaluated against gap size, d, the cut-off frequencies of the first two modes are plotted in Fig. 2*a* for a fixed waveguide height of $b = 1.6$ mm. For this analysis, $s = 6$ mm, $t = 0.017$, $a = 7.47$ mm, and $s1 = 0.75 = a/10$. As expected, for both waveguides the cut-off frequency of the first mode decreases with a decrease in the gap size, but the T-ridge waveguide displays a significantly lower cut-off frequency for a given value of d. The cut-off frequency of the second mode for the T-ridge waveguide also increases with a decrease in the gap size, while the ridge waveguide displays a normal decrease. Note that in both cases, the cut-off frequency of the first mode is substantially lower than for normal rectangular guide.

In terms of the ridge width, s, cut-off frequencies for the first two modes are shown in Fig. 2*b*. Here $a = 7.47$ mm, $b = 1.6$ mm, $d = 0.5b$, and $s1 = 0.75$ mm. The cut-off frequency of the fundamental mode for the ridge waveguide has a local minimum when the ratio s/a ; 0.5 mm. The T-ridge waveguide cut-off frequency for mode 1 on the other hand decreases gradually with an increase in s over the simulated range of 1 mm $\leq s \leq$ 6 mm. It is also shown that for this range of variation, the T-ridge waveguide achieves a lower cut-off frequency with the difference becoming more pronounced as s increases. However, for $s > 4$ mm the spacing between the first two modes reduces substantially for the T-ridge guide.

Finally, for the T-ridge waveguide with fixed dimensions $b = 1.6$ mm, $a = 7.47$ mm, $s = 6$ mm, and $d = 0.5b$, Fig. 2*c* shows that the cut-off frequencies of the first two resonant modes increase gradually with an increase in the width of the T-ridge leg width, $s1$. This is observed for a variation in the range of 0.5 mm $\leq s1 \leq 6$ mm. At $s1 = 6$ mm, the structure becomes a full ridge waveguide.

The graphs of the cut-off frequencies of the two topologies discussed in this section show that a T-ridge waveguide can achieve lower cut-off frequencies than a conventional ridge waveguide for the same outer dimensions of the waveguide. It also offers a very direct SIW implementation, as will be seen in the following section. The graphs also offer a guideline to dimensional changes that will aid in extending the stopband.

3 Pedestal SIW resonators

A T-ridge waveguide can be used to construct a resonator by shorting both ends of a half-wave section, in the same way as normal waveguides. An alternative procedure, which yields a smaller, rectangular resonator, is proposed here. This is based on the fact that, for a normal waveguide, the resonance frequencies for TE_{m0p} modes for a resonator of width a and length d are

$$\omega_{r(m0p)} = \frac{1}{\sqrt{\mu\epsilon}}\sqrt{\left(\frac{m\pi}{a}\right)^2 + \left(\frac{p\pi}{d}\right)^2} = \sqrt{\omega_{c(m0)}^2 + \omega_{c(p0)}^2}$$

where $\omega_{c(m0)}$ and $\omega_{c(p0)}$ are the cut-off frequencies of guides with widths of, respectively, a and d. If, instead of short circuiting the end walls of the waveguide, they are terminated with open circuits, a resonance mode with $p = 0$ is obtained. The resonance frequency of this mode is equal to the cut-off frequency of a guide with width a, which is significantly lower than that of the normal shorted case. If this procedure is applied to the T-ridge guide, an open circuit termination can be approximated by terminating the guide in the longitudinal direction by open guides of the same outer dimensions as that enclosing the T-ridge guide, as the effective characteristic impedance of the T-ridge guide is significantly lower than that of the open guide. As this is not an ideal open circuit, the resonant frequency of the lowest resonant mode of the whole structure is not constant with respect to length, but turns out to be an almost linear function of the ridge section length, and insensitive to the length of the open guide sections. This is very useful, as the resonant frequency can be easily controlled by setting the length of the T-ridge section. Finally, the resonant frequency can be lowered even further by reducing the length of the T-ridge leg, until the leg becomes a square post. Parametric studies of this structure, with attention to additional parameters such as Q-factor, have shown that a square structure typically yields optimal results, with small perturbations in the length allowed for fine frequency tuning.

The procedure thus results in a pedestal structure with a square or rectangular top. This structure retains the basic relationship between the cut-off frequencies of the first two modes, resulting in proportionally widely spaced resonant frequencies of the first two resonant modes. The structure also retains the miniaturisation advantages of the T-ridge guide as compared with normal dielectric filled waveguide or standard SIW guide. Finally, the pedestal structure lends itself admirably to implementation in SIW, as shown in Figs. 3*a* and *b*.

It should be noted that a similar structure was proposed in [18], but developed from a very different perspective, namely the folding of normal guides in two dimensions. While this is an elegant

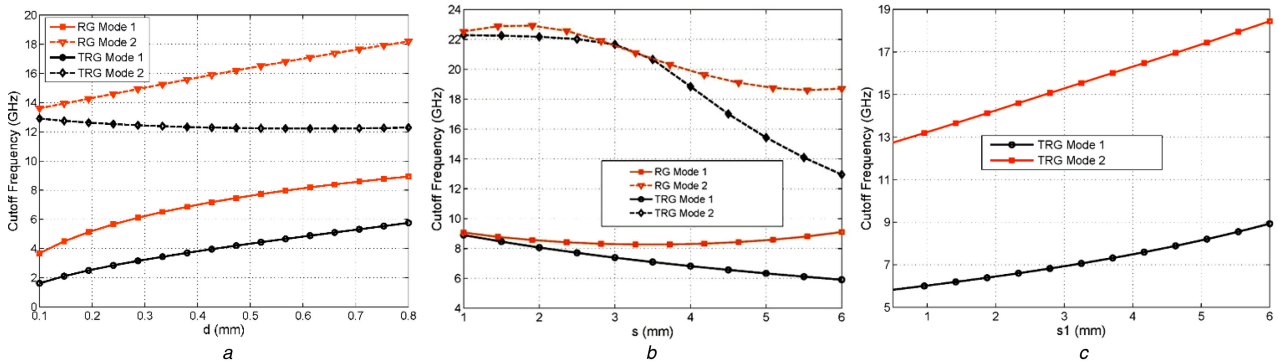

Fig. 2 *Cut-off frequencies of modes 1 and 2 versus*
(a) Gap size d, ***(b)*** Tidge width s, ***(c)*** T-ridge leg width, $s1$

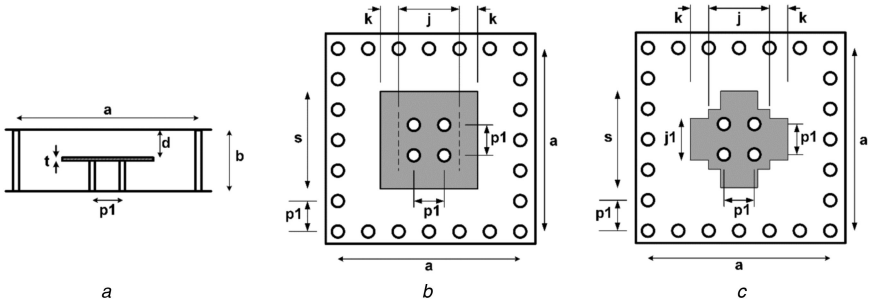

Fig. 3 *Side view and top view of SIW pedestal resonator*
(a) Side view of rectangular SIW pedestal resonator, ***(b)*** Top view of rectangular SIW pedestal resonator, ***(c)*** Top view of cross-shaped SIW pedestal resonator

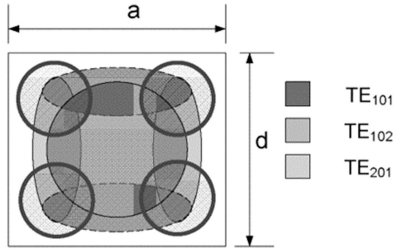

Fig. 4 *Areas of high electric field intensity for the first three resonant modes of a square pedestal resonator*

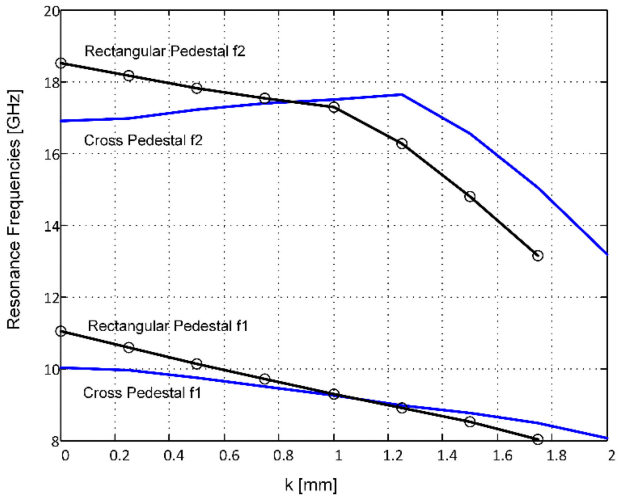

Fig. 5 *Resonant frequencies of modes 1 and 2 versus k*

approach, it does not offer much insight into the advantages of the structure, and the design is by optimisation only. In comparison, the development from a T-ridge waveguide structure allows for a much more direct correlation with the cut-off frequencies of the different modes. A related structure, using SIW techniques to create an effective metal insertion into a waveguide, was also proposed in [19]. This structure is however based on a perturbed waveguide model.

Two alternative models can also be considered for the structure proposed in this paper, namely that of a very high impedance vertical coaxial line top loaded with a very large capacitance, or that of an evanescent waveguide loaded by a capacitive obstacle. Neither of these two approaches however yield accurate models of the actual structure.

Additional improvements to the structure to separate adjacent resonant modes are possible. Fig. 4 shows a top view of a square resonator, with the areas of high electric field intensity for the first three resonant modes, calculated at resonance for each one, depicted using different colours. It is clear that the two higher order modes have the strongest field components on-axis, and that changing the structure in those areas will affect all the modes in the same way, i.e. reduce the total stored electric field and therefore the resonance frequency. If however the corner sections are removed, the fundamental mode will suffer a bigger disturbance than the higher order modes, increasing the resonant frequency separation. The resulting shape is a cross-shaped pedestal, the SIW implementation of which is shown in Fig. 3*c*.

Following, the performance of the two types of resonator is compared in terms of the resonant frequencies and the unloaded quality factors attainable by each cavity, using the eigenmode solver of CST Microwave Studio. Note that in both cases, the structure is allowed to become rectangular. The parameter k influences the length of the top of each resonator, while s denotes the width. To have both resonators display resonance for mode 1 in the same range, they are slightly different in size. For both resonators, Rogers RO4003C is used as substrate, with a height of 0.5 mm, relative permittivity of 3.38, copper thickness of 0.017 mm, and loss tangent of 0.0027 (constant versus frequency). The basic structure for both resonators therefore has $b = 1$ mm, $t = 0.017$ mm, $p1 = 1.4$ mm, via diameter = 1 mm, $d = 0.5$ mm, and $j = 2.8$ mm. The rest of the dimensions are

$$\begin{aligned} &\text{Rectangular resonator:} && a = 7.5\,\text{mm}, s = 5.0\,\text{mm} \\ &\text{Cross}-\text{shaped resonator:} && a = 7.9\,\text{mm}, s = 5.4\,\text{mm}, j1 = 3.2\,\text{mm} \end{aligned}$$

Note that the rectangular resonator is overall smaller than the cross-shaped one, for roughly the same range of resonant frequencies. The resonant frequencies of the first two modes for both resonators are shown in Fig. 5, as a function of parameter k. It is clear that while the rectangular resonator shows a bigger change in the frequency of mode 1, the frequency of mode 2 also reduces quite rapidly. The ratio is also shown in Fig. 6*a*, where the two frequencies are plotted against each other. To put this performance into perspective, the ratios of the first two resonant frequencies for a number of standard resonators are also shown in the figure, specifically those for a half-wave stripline resonator, a ring resonator, and a rectangular dielectric filled waveguide (equivalent to standard SIW guide), all realised on the same substrate.

As expected, the standard dielectric filled waveguide shows the smallest mode separation due to the occurrence of the TE_{20} mode, while both the half-wave stripline and ring resonators show a ratio of 1:2. The two new pedestal SIW resonators lie in between these two boundaries, with the cross-shaped one showing almost a 1:2 ratio at 9 GHz. In absolute terms, the increase in pass-band separation for the pedestal structures is between 3 and 4 GHz more than that of the standard guide. Empiric studies have also shown that for most cases, at least one of the pedestal structures can always be optimised to yield a ratio of very close to 1:2.

A very important distinguishing factor between these resonators is the unloaded quality factor (Q-factor). Using the same set of resonators as in the previous figures, the Q-factor for each one is calculated at resonance, using the CST eigenmode solver. Note that this solver ignores all losses when determining the resonant frequencies, but then uses the ideal fields to calculate metal surface losses and dielectric losses in a post-processing step. For these calculations, all metal parts were assumed to be copper, with a conductance of $5.8 \cdot 10^7$, and the substrate as stated before. This yields an upper bound for the Q-factor in each case, as no surface roughness is included. Fig. 6*b* shows the results of the set of analyses.

As expected, the rectangular dielectric filled guide shows the highest Q-factor, while the half-wave stripline shows the lowest. It

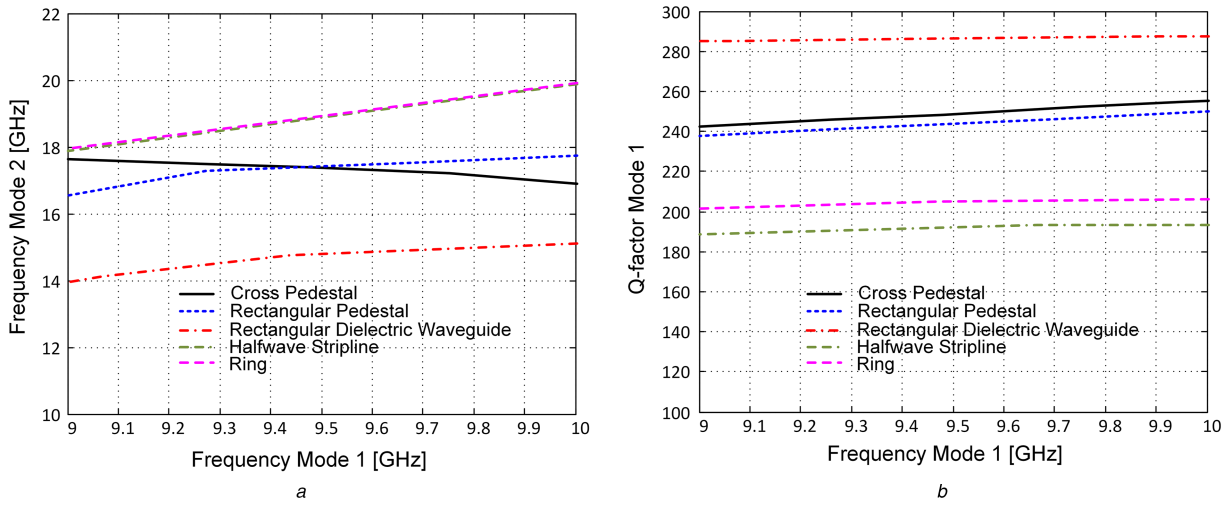

Fig. 6 *Band separation and Q of various resonators*
(a) Resonant frequency of mode 2 versus that of mode 1, ***(b)*** Q-factors of mode 1 versus frequency

Table 1 Footprint dimensions of various resonators

Half-wave stripline (50 Ω)	8.8 × 1.5
Ring resonator (50 Ω)	6.0 × 6.0
Rectangular dielectric filled waveguide	13.2 × 12.34
Rectangular pedestal	8.0 × 8.0
Cross-shaped pedestal	8.4 × 8.4

is clear that the pedestal resonators achieve Q-values which are significantly higher than the half-wave stripline, as well as the ring resonator, but fall short of the standard guide. It should be noted that the difference between the line-based resonators and the waveguide-based resonators will increase when a better substrate is used, as the former are more affected by conductor loss.

In terms of relative size, the footprints of the various resonators are shown in Table 1, all for a resonance frequency of mode 1 of 9 GHz, and all for a substrate height of 1 mm. Note that for the stripline and ring resonators, the footprint dimensions only include the metal lines. In practice, the footprint will include a certain amount of spacing around the metal strips, typically two to three times the substrate height.

It is clear that the pedestal resonators achieve a good compromise between size, Q-factor, and the ratio of the first two resonant modes.

4 X-band filter using proposed resonator

To illustrate the usage of the proposed resonators, two fourth-order filters were designed. The first, denoted as filter A, uses the cross-shaped pedestal resonator to implement a filter with a centre frequency of 9.1 GHz and a fractional 3 dB bandwidth of 4%. A standard inline coupled-resonator design is obtained from tables for a 0.01 dB ripple Chebyshev prototype, and the bandwidth scaled to yield the following k-and q-values: $q_1 = q_2 = 26$, $k_{12} = k_{34} = 0.029$, and $k_{23} = 0.0217$. The inline configuration is implemented in a square layout of four resonators, with no cross-couplings. The second filter, filter B, uses almost the same outer dimensions, but increased resonator loading through the use of the square pedestal, to implement a filter with a centre frequency of 7 GHz and a 20 dB equi-ripple return loss bandwidth of 200 MHz (or 2.9%). This filter also utilises a square layout of resonators, but with one negative cross-coupling between resonators 1 and 4, for increased stopband roll-off. Again following classical coupled-resonator design for this filter, but allowing for one negative cross-coupling, and with an additional specification of a high-end attenuation of better than 48 dB at 7.27 GHz, k-and q-values are obtained as $q_1 = q_2 = 35.5$, $k_{12} = k_{34} = 0.0246$, $k_{23} = 0.0203$, and $k_{14} = -0.00195$.

The two filters were chosen to illustrate the flexibility offered by this topology, especially in terms of ease of input coupling, implementation of cross-coupling, and the ability to have the same space envelope for quite a wide range of centre frequencies. Both were designed for Rogers RO4003 substrate, with a thickness of 0.508 mm and a loss tangent of 0.0027.

The first phase in the realisation of a prototype is the construction of the resonator, in two steps. In step one, for a given substrate, the via diameter and spacing $p1$ are determined to realise an SIW guide in the correct frequency range (here 1 mm diameter and 1.4 mm spacing). Following, the cross-section of the guide is determined using a 2D electromagnetic solver such as CST Microwave Studio. Here, values for the parameters a and s are determined, with $s1$ calculated from the via spacing and diameter. Alternatively, a single via can also be used as the post of the pedestal. Note that a single solution does not exist in this case – the designer must find an optimum compromise between size and mode separation for the specifications. The length of a rectangular resonator is then determined for resonance at the correct frequency, in this case using a 3D electromagnetic solver. The phase is completed by a choice between a rectangular topology and a cross-shaped topology, and if required, a short manual optimisation of the parameters s, k, and $j1$, in order to give a good compromise between Q-factor, size, and mode separation. Note that parameter j is calculated to just enclose the vias forming the base of the pedestal. While the design of the resonator requires the optimum determination of various dimensions, this is no different from all modern filter designs, where 3D electromagnetic simulators are used to optimise the dimensions for best usage of space.

Once the resonator is fixed dimensionally, the filter design progresses systematically using the classical S_{11} group delay tuning procedure by Ness. First, one resonator is coupled to an external port, and the spacing dimensions determined to yield the correct S_{11} group delay as calculated from design parameter q_1. Again, this process requires a full 3D electromagnetic solver. In this step, the resonator dimensions typically need to be changed slightly to compensate for the frequency shift caused by the external loading. Following, the second resonator is introduced and coupled to the first – here by means of aperture coupling in the normal waveguide manner, where in this case the aperture is set by the gap between two vias in the via wall separating the two resonators, and/or the spacing between the two resonators. Again using an iterative approach based on results from electromagnetic simulation, the coupling gap is determined to yield the S_{11} group delay as calculated from design parameter k_{12}. As in the previous step, this step also typically requires small adjustments to the resonator.

This process is then continued until the full filter without cross-couplings has been realised. The final step is introducing a cross-coupling, and adjusting the dimensions of the coupling, as well as the two resonators affected by the coupling. Note that in each case, only one or two dimensions are typically changed – nowhere in the process is an optimisation performed using all the variables. This process typically yields filters with small errors in frequency and/or

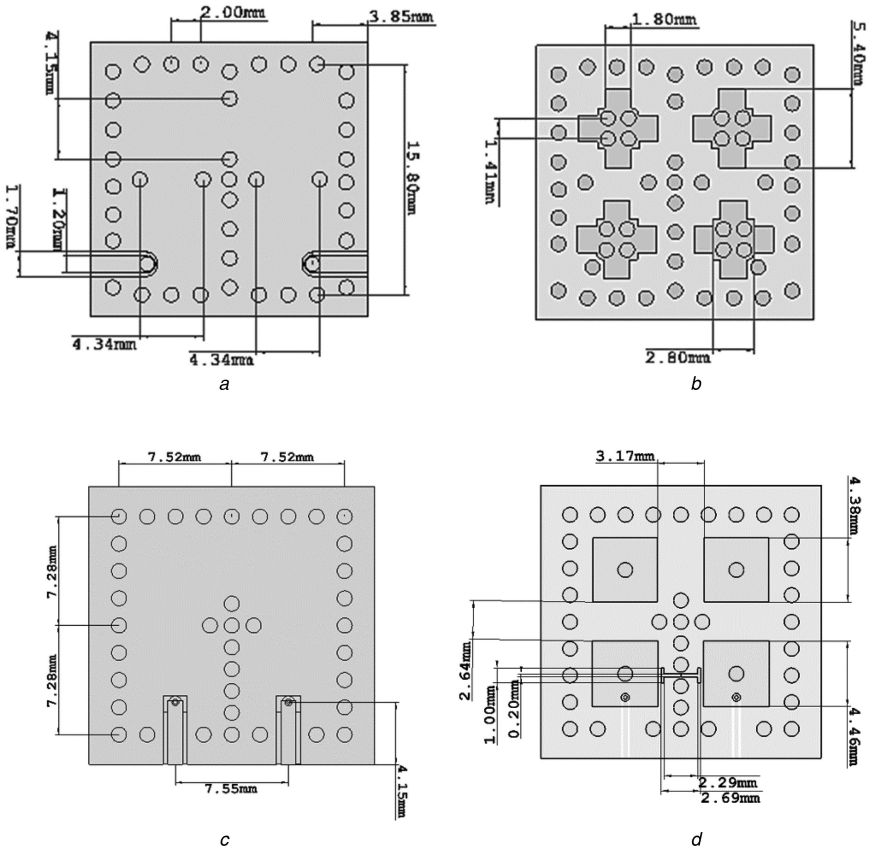

Fig. 7 *Filter Layouts*
(a) Filter A top layer, ***(b)*** Filter A internal layer, ***(c)*** Filter B top layer, ***(d)*** Filter B internal layer

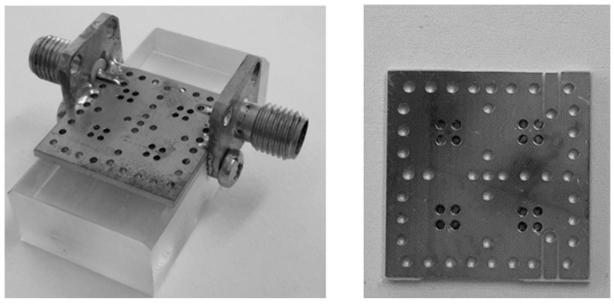

Fig. 8 . *Filter A constructed*
(a) Perspective view, ***(b)*** Top view

return loss – in the order of 1–2%. If more accurate responses are required, a full 3D optimisation can be performed as a final step. For the case of filter B, this required 31 analysis steps, optimising three variables only.

The two-layer implementation of the final structure of filter A is shown in Figs. 7*a* and *b*. The resonators are coupled to each other using magnetic coupling. The input and output couplings are also magnetic, by means of a post-transitioning from a co-planar feed line on the top layer, and shorted at the bottom ground plane. The total outside dimensions of the filter are 16.8×16.8 mm, not including the board edges.

Filter A was constructed, with the final filter shown in Fig. 8. An Agilent PNA-X was used for the verification. For measurement purposes, very simple SubMiniature version A (SMA) transitions were used as shown, with a loose shielding wall (not shown) between the connectors to prevent direct coupling between them. In use, the filter will be mounted face-down on a base in the manner of flip-chips, with the ground section connected to the ground of the base, which should ensure almost perfect isolation between the ports. The measurement results are compared with the full-wave electromagnetic simulation results in Fig. 9. A centre frequency for the main pass-band of 9.4 GHz is achieved, 113 MHz above that of the simulated response. The insertion loss of the measured filter is 4.7 dB at the centre frequency, compared with the simulated value of 2.4 dB. This is due to the fact that no surface roughness was included in the simulation. The measured 3 dB bandwidth of 365 MHz (3.9%) is very close to the simulated bandwidth of 368 MHz. Reflection is below −14 dB in the band 9.277–9.485 GHz. The measured second pass-band peak is at 18.23 GHz, or $1.94f_0$. This constitutes an absolute pass-band separation of 8.8 GHz.

The layout for filter B is shown in Figs. 7*c* and *d*. Due to the stronger loading of the resonators created by the square pedestals, almost the same outer dimensions are achieved, even though the centre frequency is 2 GHz lower. To realise the filter in a square layout, the coupling between resonators 2 and 3 can only be changed by changing the waveguide dimensions. In comparison, the cross-shaped pedestal allowed for the extension of the pedestal top in a rectangular (i.e. not square) fashion to obtain closer proximity without changing the waveguide dimensions. Note also the inductive feed which passes through the pedestal tops of resonators 1 and 4 to achieve the desired level of input coupling. The negative cross-coupling between resonators 1 and 4 is achieved very simply by an etched T-section. It should be noted that the simplicity of such a coupling is a distinct advantage of this topology.

The filter was simulated in CST with lossy metal and lossy dielectric, and the results are shown in Fig. 10. As a short full optimisation was performed, the return loss performance is almost exact, with −19.8 dB achieved over the design bandwidth of 6.9–7.1 GHz. An insertion loss of 1.8 dB is predicted in the centre of the band. The attenuation is as designed, with the asymmetry between low-band and high-band attenuation due to the frequency dependence of the cross-coupling and the frequency behaviour of waveguide cavities. This is standard for waveguide cavities of any technology. A better than 40 dB spurious-free attenuation is predicted from 7.2 to 15.5 GHz, with the main second pass-band centred at 16.24 GHz, or $2.32f_0$.

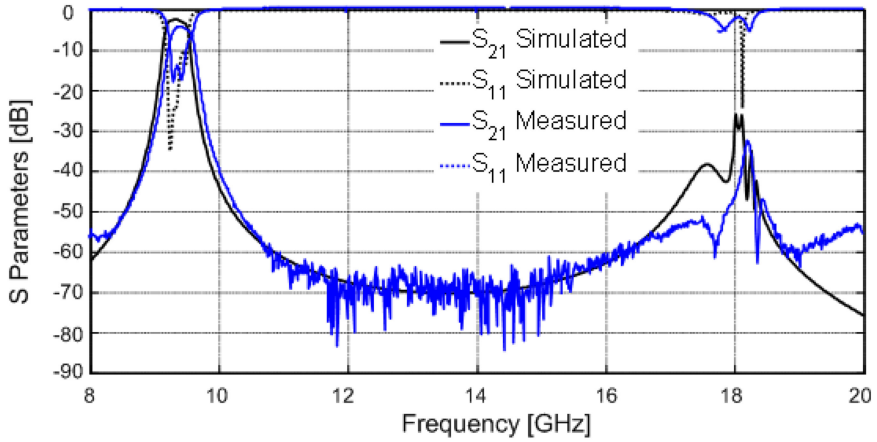

Fig. 9 *Broadband measurement results for filter A*

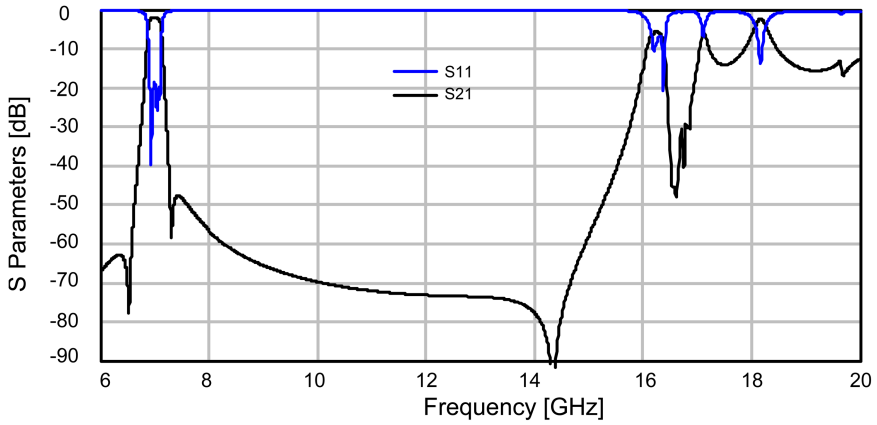

Fig. 10 *Broadband simulation results for filter B*

The results of the two filters can be compared with existing solutions. In [2], full-sized microstrip and coplanar waveguide resonators are loaded with complementary split ring resonators (CSRRs). Two third-order filters, one at $f_0 = 1.8$ GHz and one at $f_0 = 2.4$ GHz, both with 10% relative bandwidth, achieve stopbands of better than 20 dB over, respectively, 5 and 8 GHz. In [20], a so-called 'butterfly resonator' is used in a single resonator low-pass filter with a cut-off of 1 GHz. This resonator achieved a very small size of 0.1 of a wavelength, and attenuation of 17 dB from 2.37 to18 GHz. The author also provided a useful table of other planar resonators and their performance. While the stopbands of these filters are all very wide, they are all non-waveguide solutions, with lower Q-values than waveguide. In many cases, the resonators effectively approximate lumped elements, which accounts for the very wide stopbands. In terms of waveguide solutions, Salehi and Mehrshahi [14] uses dissimilar oversized SIW cavities with slot loading to design two filters at $f_0 = 10$ GHz and better than 30 dB attenuation stopbands of up to 19 GHz. In [21, 22], authors use cross-coupling of normal or higher-order modes to create transmission zeros distant from the pass-band, with, respectively, a 50 dB attenuation stopband achieved between 27.5 and 31.3 GHz for a fourth-order filter with a pass-band of 19.2 to 21.2 GHz, and a 50 dB attenuation stopband of 0–10 GHz achieved for a third-order filter with a 1 GHz bandwidth at $f_0 = 13$ GHz.

The most similar solutions to the structure proposed in this paper, are those in [23–25]. In [23], waveguides are loaded dielectrically to reduce size, achieving a fourth-order Chebyschev filter, measuring $40 \times 40 \times 12$ mm, with $f_0 = 3.8$ GHz, a bandwidth of 3%, insertion loss of 0.4 dB, and better than 70 dB attenuation over the band 2.3–3.6 GHz, and better than 20 dB attenuation over the band 4–5 GHz. Both [24, 25] use CSRRs to load SIW cavities, and, respectively, achieve a filter with transverse dimensions of 70×20 mm, with $f_0 = 5$ GHz, a 3 dB bandwidth of 320 MHz, insertion loss of 3.9 dB, and an attenuation of better than 40 dB from 5.5 to 6.5 GHz, and a filter with transverse dimensions of 45×12 mm, with $f_0 = 5.45$ GHz, a 3 dB bandwidth of 187 MHz, insertion loss of 5.8 dB, and an attenuation of better than 45 dB to up to 9 GHz. It should be clear that the proposed filters offer smaller footprints, similar insertion loss, and a wider stopband.

5 Conclusions

Pedestal SIW resonators are proposed which utilise the mode separation characteristics of ridge surface integrated waveguide, specifically T-ridge SIW guide. Two shapes of the pedestal resonator are compared with standard resonators, and are shown to offer a good compromise between size, Q-factor, and mode separation. Two fourth-order filters are designed in PCB multilayered technology and performance verified by both simulation and/or measurement. The results show improved performance over published filters employing similar miniaturisation techniques.

6 Acknowledgments

The authors thank Reutech Radar Systems (Pty) Ltd for financial support of this project, and CST GmbH for the use of CST Microwave Studio.

7 References

[1] Nassar, S., Meyer, P., Van der Walt, P.W.: 'An S-band combline filter with reduced size and increased pass-band separation'. 14th Conf. on Microwave Techniques (COMITE 2015), Pardubice, 2015

[2] García-García, J., Martín, F., Falcone, F., *et al.*: 'Microwave filters with improved stopband based on sub-wavelength resonators', *IEEE Trans. Microw. Theory Tech.*, 2005, **55**, (6), pp. 1104–1113

[3] Djerafi, T., Aubert, H., Wu, K.: 'Ridge substrate integrated waveguide (RSIW) dual-band hybrid ring couplers', *IEEE Microw. Wirel. Compon. Lett.*, 2012, **22**, pp. 70–72

[4] Kazemi, R., Fathy, A.E.: 'Design of a wideband eight-way single ridge substrate integrated', *IET Microw. Antennas Propag.*, 2015, **7**, pp. 648–656

[5] Yang, F., Liu, R., Yu, H.: 'Canonical ridged SIW filters in LTCC'. Int. Conf. on Microwave Technology Computational Electromagnetics (ICMTCE), 2011

[6] Mallahzadeh, A.R., Esfandiarpour, S.: 'Wideband H-plane horn antenna based on ridge substrate integrated waveguide', *IEEE Antennas Wirel. Propag. Lett.*, 2012, **11**, pp. 85–88
[7] Helszajn, J.: '*Ridge waveguides and passive microwave components (IEE electromagnetic wave series 49)*' (Institution of Engineering and Technology, 2000)
[8] Bornemann, J., Arndt, F.: 'Transverse resonance, standing wave, and resonator formulations of the ridge waveguide eigenvalue problem and its application to the design of E-plane finned waveguide filters', *IEEE Trans. Microw. Theory Tech.*, 1990, **38**, pp. 1104–1113
[9] Marcuvitz, N.: '*Waveguide handbook*' (P. Peregrinus, 1951)
[10] Hoefer, W.J., Burton, M.N.: 'Closed-form expressions for the parameters of finned and ridged waveguides', *IEEE Trans. Microw. Theory Tech.*, 1982, **30**, pp. 2190–2194
[11] Hopfer, S.: 'The design of ridged waveguides', *IRE Trans. Microw. Theory Tech.*, 1955, **3**, pp. 20–29
[12] Chen, X.P., Wu, K.: 'Substrate integrated waveguide filter: basic design rules and fundamentals', *IEEE Microw. Mag.*, 2014, **15**, pp. 108–116
[13] Wu, K.: 'Integration and interconnect techniques of planar and non-planar structures for microwave and millimeter-wave circuits – current status and future trend'. IEEE Asia Pacific Microwave Conf., APMC, 2001
[14] Salehi, M., Mehrshahi, E.: 'Spurious-response suppression of substrate integrated waveguide filters using multishape resonators and slotted plane structures', *Int. J. RF Microw. Comput.-Aided Eng.*, 2011, **2**, (6), pp. 650–657
[15] Hao, Z., Hong, W., Chen, J.*, et al.*: 'Compact super-wide bandpass substrate integrated waveguide (SIW) filters', *IEEE Trans. Microw. Theory Tech.*, 2005, **53**, (9), pp. 2968–2977
[16] Wang, J., Hong, W., Tang, H.*, et al.*: 'Ultra-wide band bandpass filter with multiple frequency notched bands based on SIW and SIR technology'. 2009 European Microwave Conf. (EuMC), Rome, September 2009, pp. 268–271
[17] Bozzi, M., Winkler, S.A., Wu, K.: 'Broadband and compact ridge substrate-integrated waveguides', *IET Microw. Antennas Propag.*, 2009, **4**, (11), pp. 1965–1973
[18] Lin, H.: 'Novel folded resonators and filters'. IEEE/MTT-S Int. Microw. Symp., 2007
[19] Li, L., Wei, Q.-F., Li, Z.-F.*, et al.*: 'Compact concavo-convex cavity filters using multilayer substrate integrated waveguide', *Electron. Lett.*, 2011, **47**, (8), pp. 500–502
[20] Dou, Y., Wang, J., Cui, H.*, et al.*: 'Miniaturized microstrip lowpass filter with ultra-wide stopband', *ACES J.*, 2013, **28**, (7), pp. 640–645
[21] Chen, X.P., Wu, K., Drolet, D.: 'Substrate integrated waveguide filter with improved stopband performance for satellite ground terminal', *IEEE Trans. MTT*, 2009, **57**, (3), pp. 674–683
[22] Zhang, P.J., Li, M.Q.: 'Substrate integrated waveguide filter with improved stopband performance using LTCC technology', *Prog. Electromagn. Res. C*, 2014, **54**, pp. 155–162
[23] Nocella, V., Pellicia, L., Tomassoni, C.*, et al.*: 'Ultra-compact high-performance filters based on TM dual-mode dielectric-loaded cavities', *Int. J. Microw. Wirel. Technol.*, 2014, **6**, (2), pp. 151–159
[24] Jiang, W., Shen, W., Zhou, L.*, et al.*: 'Miniaturized and high-selectivity substrate integrated waveguide (SIW) bandpass filter loaded by complementary split-ring resonators (CSRRs)', *J. Electromagn. Waves Appl.*, 2012, **26**, (11-12)
[25] Dong, Y.D., Yang, T., Itoh, T.: 'Substrate integrated waveguide loaded by complementary split-ring resonators and its applications to miniaturized waveguide filters', *IEEE Trans. Microw. Theory Tech.*, 2009, **57**, (9), pp. 2211–2223